

REPORT DOCUMENTATION PAGE

AFRL-SR-AR-TR-05-

Public reporting burden for this collection of information is estimated to average 1 hour per response, including the time for reviewing instructions, searching existing data sources, gathering the required data, reviewing the collected data, completing and reviewing this collection of information. Send comments regarding this burden estimate or any other aspect of this collection of information, including suggestions for reducing this burden, to Washington Headquarters Services, Directorate for Information Operations and Reports (0704-0188), 1215 Jefferson Davis Boulevard, Arlington, VA 22202-4302. Respondents should be aware that notwithstanding any other provision of law, no person shall be subject to any penalty for failing to comply with a collection of information if it does not have a valid OMB control number. **PLEASE DO NOT RETURN YOUR FORM TO THE ABOVE ADDRESS.**

1. REPORT DATE (DD-MM-YYYY) 9/16/05		2. REPORT TYPE Final Performance		3. DATES COVERED (From - To) 9/1/01 - 8/31/03	
4. TITLE AND SUBTITLE Simulations of High-Speed Cavity Flows in a Scramjet Engine by the CESE Method				5a. CONTRACT NUMBER F49620-01-1-0051	
				5b. GRANT NUMBER	
				5c. PROGRAM ELEMENT NUMBER	
6. AUTHOR(S) Sheng-Tao John Yu, Chang-Kee Kim, and Zengchan Zhang				5d. PROJECT NUMBER	
				5e. TASK NUMBER	
				5f. WORK UNIT NUMBER	
7. PERFORMING ORGANIZATION NAME(S) AND ADDRESS(ES) Mechanical Engineering Dept. The Wayne State Univ. 5050 Anthony Wayne Drive Detroit, MI 48202				8. PERFORMING ORGANIZATION REPORT NUMBER	
9. SPONSORING / MONITORING AGENCY NAME(S) AND ADDRESS(ES) Dr. John Schmisseeur AFOSR/NA DSN 426-6962 E-Mail: john.schmisseeur@afosr.af.mil				10. SPONSOR/MONITOR'S ACRONYM(S)	
				11. SPONSOR/MONITOR'S REPORT NUMBER(S)	
12. DISTRIBUTION / AVAILABILITY STATEMENT Approved for public release; distribution unlimited					
13. SUPPLEMENTARY NOTES					
14. ABSTRACT In this report we summarize numerical results of supersonic flows over open cavities in the setting of a dual-mode ramjet/scramjet engine. To calculate the unsteady cavity flows, we employ the Space-Time Conservation Element and Solution Element (CESE) method, a novel numerical method based on a unified treatment of space and time in calculating flux balance. Supersonic cavity flows with and without fuel injection are studied to understand the mechanisms of mixing enhancement and flame holding by cavities. Without injection, numerical results compared favorably with the experimental data for dominant frequencies and time-averaged pressure coefficients inside the cavities. With an upstream injection, the flow oscillations are drastically suppressed. In a downstream injection arrangement, cavity-generated acoustic waves and vortices greatly enhance fuel/air mixing. Numerical results show that the CESE method provides high-fidelity numerical results of unsteady flows in the advanced scramjet engine concept.					
15. SUBJECT TERMS Scramjet engine, hypersonic propulsion					
16. SECURITY CLASSIFICATION OF:			17. LIMITATION OF ABSTRACT	18. NUMBER OF PAGES	19a. NAME OF RESPONSIBLE PERSON Sheng-Tao John Yu
a. REPORT	b. ABSTRACT	c. THIS PAGE			19b. TELEPHONE NUMBER (include area code) 614-2920-2902

Simulation of High-Speed Cavity Flows in a Scramjet Engine by the Space-Time CESE Method

**The final report for
AFSOR, USAF, under grant number F49620-01-1-0051**

By

S.-T. John Yu*, Chang-Kee Kim, and Zeng-Chan Zhang

Mechanical Engineering Department

The Wayne State University

Detroit, Michigan 48202

*** Current address of the corresponding author:**

The Mechanical Engineering Department

The Ohio State University

650 Ackerman Road

Suite # 255

Columbus, OH 43202

Tel: 614-292-2902

Email: yu.274@osu.edu

DISTRIBUTION STATEMENT A
Approved for Public Release
Distribution Unlimited

20051114 016

Summary

In this report we summarize numerical results of supersonic flows over open cavities in the setting of a dual-mode ramjet/scramjet engine. To calculate the unsteady cavity flows, we employ the Space-Time Conservation Element and Solution Element (CESE) method, a novel numerical method based on a unified treatment of space and time in calculating flux balance. Supersonic cavity flows with and without fuel injection are studied to understand the mechanisms of mixing enhancement and flame holding by cavities. Without injection, numerical results compared favorably with the experimental data for dominant frequencies and time-averaged pressure coefficients inside the cavities. With an upstream injection, the flow oscillations are drastically suppressed. In a downstream injection arrangement, cavity-generated acoustic waves and vortices greatly enhance fuel/air mixing. Numerical results show that the CESE method provides high-fidelity numerical results of unsteady flows in the advanced scramjet engine concept.

The results reported here have been published in the following journal and conference papers:

1. C.-K. Kim, S.-T. J. Yu, and Z. Zhang, "Direct Calculation of High-Speed Cavity Flows in a Scramjet Engine by the CESE method," AIAA J., vol. 42, no. 5 (2004) pp. 912-919.
2. Z. Zhang, S.-T. J. Yu and S.-C. Chang, "A Space-Time Conservation Element and Solution Element Method for Solving the Two- and Three-Dimensional Euler Equations by Quadrilateral and Hexahedral Meshes," Journal of Computational Physics, vol. 175, no.1 (2002) pp 168-199.
3. C.-K. Kim, K.-S. Im and S.-T. J. Yu, "Numerical Simulation of Unsteady Flows in a Scramjet Engine by the CESE Method," AIAA 2002-3887, the 38th AIAA/ASME/SAE/ASEE Joint Propulsion Conference, June 2002, Indianapolis, IN.
4. C.-K. Kim and S.-T. J. Yu, "Numerical Simulation of Supersonic Cavity Flows in a Scramjet Engine by the CESE Method," the JANNAF Meeting, Aero Propulsion, June 2002, Destin, FL.
5. C.-K. Kim, K.-S. Im and S.-T. J. Yu, "Simulation of High-Speed Cavity Flows in a Scramjet Engine by the CESE Method," AIAA 2002-1084, the 40th Aerospace Sciences Meeting and Exhibit, January 2002, Reno, NV.

Table of Content

1. Introduction	4
2. Governing Equations	7
2.1 Mixtures of Thermally Perfect Gases	7
2.2 Governing Equations	11
2.3. Jacobian Matrix of Flux Functions	13
2.4 Evaluation of Thermodynamic/Chemical Parameters	25
2.5 Flow Equations in Multi-Dimensional Space	30
3. The CESE Method	33
4. Results and Discussions.....	39
4.1 Frequency Calculations	39
4.2 Pressure Amplitude Calculation	41
4.3 Cavity for Fuel/Air Mixing Enhancement	42
5. Concluding Remarks	44
Acknowledgement.....	45
References	47
Figure Captions.....	49

1. Introduction

Fuel injection, ignition, and flameholding are challenging issues for high-speed combustion. In a viable scramjet engine, the fuel injection method employed must provide rapid fuel/air mixing with minimum total-pressure loss in the airstream. A stable flameholding system under a wide range of operating conditions is critical to sustain the supersonic combustion. Recently, cavity-based flameholders, an integrated mixing-enhancement and flameholding approach, have attracted considerable attention in the scramjet community. Under suitable conditions, flow recirculation, or the trapped vortices, significantly increases the flow residence time of the fluid entering the cavity. A pilot flame could be set up inside the cavity to provide a pool of hot chemical radicals, which in turn would reduce the ignition delay of the air/fuel mixture in airstream and thus sustain high-speed combustion.

High-speed cavity flows are inherently unsteady, involving both broadband small scale fluctuations typical of turbulent flows, as well as distinct resonance with harmonic properties in its frequencies and amplitudes. In the past, it has been demonstrated that the aspect ratio of the cavity and free stream flow conditions are the critical parameters dominating the complex flow features, including boundary layer separation, compressible free shear layer with shedding vortices, linear/nonlinear acoustic waves, and complex shock and expansion waves interacting with vortices and acoustic waves.

In the setting of wheel wells and bomb bays, previous studies for high-speed cavity flows showed that cavity flows could be categorized into the following two groups: (i) open cavity flows, when $L/D < 7\sim 10$, and (ii) closed cavity flows, when $L/D > 7\sim 10$, where L denotes the length of the cavity, and D the depth. In flows over cavities of large aspect ratios ($L/D > 7\sim 10$), the separated free shear layer emanating from the upstream corner of the cavity reattaches to the bottom wall of the cavity and results in two separated recirculation zones near the two corners between the lateral walls and the cavity floor. The resultant low pressure zones at the lower corners and high pressures on the cavity floor, where the shear layer reattaches, lead to significant drag and pressure loss of the airstream. In this case, mass addition/ejection into/from the cavity by aerodynamic unsteadiness is low to moderate, and the flow is referred to as "closed."

On the other hand, flows over cavities with smaller aspect ratios, $L/D < 7\sim 10$, result in reattachment of the free shear layer to the rear bulkhead of the cavity. The impingement of the free shear layer on the rear lateral wall causes violent unsteady motions and results in significant periodical mass addition/ejection near the rear bulkhead of the cavity, and the flows are referred to as "open." The wave patterns of open cavity flows could be further categorized into (i) transverse mode for very short cavities, $L/D \cong 1$, and (ii) longitudinal mode for longer cavities, e.g., $2\sim 3 < L/D < 7\sim 10$. In short cavities, $L/D < 2$, only one main vortex inside the cavity is sustained by the driving shear layer spanning the top of the cavity. The up and down motions of the single main recirculation bubble generate acoustic waves, which by and large propagate in the direction perpendicular to the free shear layer, provided the free stream is transonic. The propagating waves are referred to as in a transverse mode. On the other hand, when the cavity is longer, $2\sim 3 < L/D < 7\sim 10$, multiple moving vortices occur inside the cavity leading to complex interactions among trapped vortices, propagating and rebounding pressure waves, and the flapping free shear layer. In general, the rebounding pressure waves, while interacting with the free shear layer, drastically amplify the growth rate of the free shear layer, which in turn sheds enormous vortices propagating towards and impinging on the aft wall of the cavity. Due to propagating vortices in the streamwise direction and the rebounding pressure waves, prevalent acoustic waves propagate in the longitudinal direction outside the cavity into the downstream area. If the airstream is transonic or subsonic, the acoustics would transversely propagate into the upstream areas.

In the setting of supersonic combustion inside a scramjet engine, trapped vortices inside cavities could be useful for flame holding. Moreover, cavity resonance, which produces periodic mass addition/expulsion with large flow structures, could be useful for mixing enhancement. Simultaneously, cavity drag must be minimum, e.g., much less than that of a bluff body, and thus only causes acceptable pressure loss. Gruber et al. [1, 2] have developed a dual-mode ramjet/scramjet engine concept, which is envisioned to use hydrocarbon fuels for a flight regime of Mach numbers from 3 to 6 ~ 9. In their supersonic combustors [1, 2], open cavities with aspect ratios about $5 < L/D < 8$ have been tested in conjunction with various fuel injection schemes. Numerical simulation of cavity flows has been conducted by Baurle et al. [3]. The results showed that the cavities have great potential to be a viable combined flameholder/mixing enhancement device for scramjet engine combustor. Similar ideas have

also been independently proposed and tested by Yu et al. [4]. In particular, Yu et al. [4] has tested supersonic flows passing multiple cavities. Some of recent results have been summarized by Ben-Yaker and Hanson [5].

In the past, extensive experimental and theoretical studies on cavity flows have been conducted for applications in wheel well and bomb bay, and flow characteristics such as the oscillation frequency and amplitudes at various locations in the cavity have been reported [6-11]. However, it is difficult to directly apply this knowledge base to cavity flows for the advanced scramjet engines due to much shorter length/time scales in scramjet engine. Additional complexity associated with fuel injection also warrants further studies because cavity flows and the associated acoustics would be drastically changed by the fuel injection schemes employed. In particular, inherent oscillations of cavity flows may be significantly suppressed by an upstream injection [4, 9-11].

In the present report, we will focus on time-accurate calculation of supersonic cavity flows in the setting of a dual mode ramjet/scramjet engine combustor [1, 2]. The objectives of the present study are: (i) to validate the numerical results by assessing the calculated frequencies and amplitudes of pressure oscillations and compared them with previous reported data; (ii) to assess the fuel/air mixing enhancement based on applying upstream as well as downstream injection to cavity flows; and (iii) to demonstrate the capabilities of the CESE method for capturing complex flow features of the supersonic cavity flows.

The rest of the report will be organized as follows. Chapter 2 reviews the model equations to be solved by the CESE method. Detailed derivation for the flow equations of the gas mixtures is presented. Chapter 3 provides background information of the CESE method. Chapter 4 shows numerical solutions, including comparison between the numerical results and previously reported data. Moreover, we will show the effects by both upstream and downstream injection on pressure oscillations, acoustics, and vortices, leading to effects on fuel/air mixing and flameholding. We then offer concluding remarks and provide cited references.

2. Governing Equations

In this chapter, comprehensive discussions are provided for the governing equations of gas mixtures. Although, two-dimensional solutions will be provided in Chapter 3, we will focus on one-dimensional equations with detailed derivation. Extension to multi-dimensional flow equations is straightforward and will only be briefly illustrated at the end of this chapter.

2.1 Mixtures of Thermally Perfect Gases

Consider a mixture of N different thermally perfect gas species, which generally are not calorically perfect, i.e., the specific heats of each species is not constant. Let the species be in thermal equilibrium with each other. As such all species share the common mixture absolute temperature T and each individual gas species i ($i = 1, 2, \dots, N$) satisfies the perfect gas law

$$P_i = \rho_i R_i T \quad (2.1)$$

Here P_i , ρ_i , and R_i are the partial pressure, the mass density, and the gas constant of species i , respectively. Note that $R_i = R_u / M_i$, $i = 1, 2, \dots, N$, with R_u and M_i , respectively, being the universal gas constant and the molecular weight of species i . In addition, it is assumed that the static pressure p of the mixture can be determined using Dalton's law, i.e.,

$$P = \sum_{i=1}^N P_i = T \sum_{i=1}^N \rho_i R_i \quad (2.2)$$

To proceed, a set of definitions is given in the following. The mass fraction of species i is

$$Y_i \stackrel{\text{def}}{=} \frac{\rho_i}{\rho} \quad (2.3)$$

where ρ is the mass density of the mixture, i.e.,

$$\rho \stackrel{\text{def}}{=} \sum_{i=1}^N \rho_i \quad (2.4)$$

Note that, by definition,

$$\sum_{i=1}^N Y_i = 1 \quad (2.5)$$

For a reason to be shown (see Eq. (2.14)),

$$R = \sum_{i=1}^N Y_i R_i \quad (2.6)$$

is referred to as the gas constant of the mixture. Let e_i and s_i , respectively, denote the specific internal energy and the specific entropy of species i . Then the specific internal energy and the specific entropy of the mixture are

$$e = \sum_{i=1}^N Y_i e_i \quad (2.7)$$

and

$$s = \sum_{i=1}^N Y_i s_i \quad (2.8)$$

respectively. Note that, because the specific internal energy of any thermally perfect gas species is a function of temperature only, each e_i is a function of T only. Let $e_i = \frac{de_i}{dT}$ for each i . Then

$$c_v = \sum_{i=1}^N Y_i \dot{e}_i > 0 \quad (2.9)$$

Replacing Y_N by $\sum_{i=1}^{N-1} Y_i$ (See Eq. (2.5)), Eq. (2.9) implies that

$$c_v = \dot{e}_N + \sum_{i=1}^{N-1} Y_i (\dot{e}_i - \dot{e}_N) > 0 \quad (2.10)$$

Using Eqs. (2.3) and (2.4), and replacing ρ_N by $\rho - \sum_{i=1}^{N-1} \rho_i$ (See Eq. (2.4)), Eq. (2.2), (2.6) and (2.7) imply that

$$p = \left[\rho R_N + \sum_{i=1}^{N-1} \rho_i (R_i - R_N) \right] T \quad (2.11)$$

$$R = R_N + \sum_{i=1}^{N-1} \frac{\rho_i}{\rho} (R_i - R_N) \quad (2.12)$$

and

$$e = e_N + \sum_{i=1}^{N-1} \frac{\rho_i}{\rho} (e_i - e_N) \quad (2.13)$$

respectively. The key conclusions that can be drawn from Eqs. (2.11)-(2.13) are given in the following. Eqs. (2.11) and (2.12) imply that

$$p = \rho RT \quad (2.14)$$

i.e., R is the gas constant of the mixture. Note that R_i , $i = 1, 2, \dots, N$, are assumed to be constant in the current study. As such, with the aid of Eq. (2.12), Eq. (2.11) implies that

$$dp = \rho R dT + TR_N d\rho + T \sum_{i=1}^{N-1} (R_i - R_N) d\rho_i \quad (2.15)$$

Because each e_i is a function of T only, Eq. (2.13) implies that e is a function of T , ρ and ρ_i , $i = 1, 2, \dots, N-1$. As such, with the aid of Eq. (2.10) and the relation $de_i = \dot{e}_i dT$, one has

$$de = c_v dT - \left[\sum_{i=1}^{N-1} \rho_i (e_i - e_N) \right] \frac{d\rho}{\rho^2} + \frac{1}{\rho} \sum_{i=1}^{N-1} (e_i - e_N) d\rho_i \quad (2.16)$$

It follows from Eq. (2.16) that

$$c_v = \left(\frac{\partial e}{\partial T} \right)_{\rho, \rho_1, \rho_2, \dots, \rho_{N-1}} \quad (2.17)$$

Because holding the value of ρ and ρ_i , $i = 1, 2, \dots, N-1$ constant is equivalent to holding the value of ρ_i , $i = 1, 2, \dots, N$ constant (see Eq. (2.4)), Eq. (2.17) implies that c_v is the specific heat of the gas mixture at constant volume. Because e is a function of T , ρ and ρ_i , $i = 1, 2, \dots, N-1$, implicitly T is a function of e , ρ and ρ_i , $i = 1, 2, \dots, N-1$. Substituting this functional relation into Eq. (2.11), one arrives at the conclusion that implicitly P is a function of e , ρ and ρ_i , $i = 1, 2, 3, \dots, N-1$, i.e.,

$$p = p^{(1)}(e, \rho, \rho_1, \rho_2, \dots, \rho_{N-1}) \quad (2.18)$$

Here $P^{(1)}$ is a function of e , ρ and ρ_i , $i = 1, 2, \dots, N-1$.

By eliminating dT and using the fact that $c_v > 0$, Eqs. (2.15) and (2.16) can be combined to yield

$$dp = \frac{\rho R de}{c_v} + \left[R_N T + \frac{R}{\rho c_v} \sum_{i=1}^{N-1} \rho_i (e_i - e_N) \right] d\rho + \sum_{i=1}^{N-1} \left[(R_i - R_N) T - \frac{R}{c_v} (e_i - e_N) \right] d\rho_i \quad (2.19)$$

From Eq. (2.19), one arrives at the conclusion that

$$p_e \stackrel{\text{def}}{=} \left(\frac{\partial p}{\partial e} \right)_{\rho, \rho_1, \rho_2, \dots, \rho_{N-1}} = \frac{\rho R}{c_v} \quad (2.20)$$

$$p_\rho \stackrel{\text{def}}{=} \left(\frac{\partial p}{\partial \rho} \right)_{e, \rho_1, \rho_2, \dots, \rho_{N-1}} = R_N T + \frac{R}{\rho c_v} \sum_{i=1}^{N-1} \rho_i (e_i - e_N) \quad (2.21)$$

And, for $i = 1, 2, \dots, N-1$,

$$p_{\rho_i} \stackrel{\text{def}}{=} \left(\frac{\partial p}{\partial \rho_i} \right)_{e, \rho, \rho_1, \rho_2, \dots, \rho_{N-1} / \rho_i} = (R_i - R_N) T + \frac{R}{c_v} (e_i - e_N) \quad (2.22)$$

Here, for any $i = 1, 2, \dots, N-1$,

$$\left(\frac{\partial p}{\partial \rho_i} \right)_{e, \rho_1, \rho_2, \dots, \rho_{N-1} / \rho_i}$$

denotes the partial derivative of p with respect to ρ_i assuming that, except ρ_i , all other parameters in the set $\{e, \rho, \rho_1, \rho_2, \dots, \rho_{N-1}\}$ are held constant. Note that an immediate result of Eqs. (2.11), (2.21) and (2.22) is

$$p \equiv \rho p_\rho + \sum_{i=1}^{N-1} \rho_i p_{\rho_i} \quad (2.23)$$

Next, we shall provide a brief discussion of the "frozen speed of sound" of a gas mixture. As a preliminary, note that by using the thermodynamic relation $s_i = s_i(T, \rho_i)$, the relation $\rho_i = \rho Y_i$, and Eq. (2.5), Eq. (2.8) implies that s is a function of T , ρ , and Y_i , $i = 1, 2, \dots, N-1$. As such implicitly T is a function of s , ρ , and Y_i , $i = 1, 2, \dots, N-1$. Substituting this functional relation into Eq. (2.14) and observing that R is a function of Y_i , $i = 1, 2, \dots, N-1$ only (see Eqs. (2.5) and (2.6)), one concludes that implicitly p is a function of s , ρ , and Y_i , $i = 1, 2, \dots, N-1$, i.e.,

$$p = p^{(2)}(s, \rho, Y_1, Y_2, \dots, Y_{N-1}) \quad (2.24)$$

Here $p^{(2)}$ is a function of s , ρ and Y_i , $i = 1, 2, \dots, N-1$. Let a_f be the frozen speed of sound of the mixture, i.e.,

$$a_f \stackrel{\text{def}}{=} \sqrt{\left(\frac{\partial p}{\partial \rho} \right)_{s, Y_1, Y_2, \dots, Y_{N-1}}} \quad (2.25)$$

Note that, because of Eq. (2.5), holding the values of Y_i , $i = 1, 2, \dots, N-1$ constant automatically implies that the value of Y_N is also held constant. As such, adding Y_N to the list of the subscripts of the partial derivative in Eq. (2.25) will have no impact on the derivative. In the following, it will be shown that

$$a_f = \sqrt{RT \left(1 + \frac{R}{c_v}\right)} = \sqrt{\frac{p}{\rho} \left(1 + \frac{p_e}{p}\right)} \quad (2.26)$$

To proceed, note that by using (i) $\rho_i = \rho Y_i$, (ii) $P_i = \rho Y_i R_i T$, and (iii) the thermodynamic relation

$$ds_i = \frac{1}{T} \left(de_i - \frac{p_i d\rho_i}{\rho_i^2} \right) \quad (2.27)$$

One concludes that

$$ds_i = \frac{e_i}{T} - \frac{R_i d\rho}{\rho} - \frac{R_i dY_i}{Y_i} \quad (2.28)$$

With the aid of Eqs. (2.6), (2.9) and (2.28), Eq. (2.8) implies that

$$ds = \frac{c_v dT}{T} - \frac{R d\rho}{\rho} + \sum_{i=1}^N (s_i - R_i) dY_i \quad (2.29)$$

Moreover, with the aid of Eq. (2.6), Eq. (2.14) implies that

$$dp = \rho R dT + RT d\rho + \rho T \sum_{i=1}^N R_i dY_i \quad (2.30)$$

By eliminating dT and using the fact that $dY_N = -\sum_{i=1}^{N-1} dY_i$ (see Eq. (2.5)), Eqs. (2.29) and (2.30) can be combined to yield

$$dp = \frac{\rho RT}{c_v} ds + RT \left(1 + \frac{R}{c_v}\right) d\rho + \rho R \sum_{i=1}^{N-1} \left[\left(1 + \frac{R}{c_v}\right) (R_i - R_N) - \frac{R}{c_v} (s_i - s_N) \right] dY_i \quad (2.31)$$

An immediate result of Eq. (2.31) is

$$\left(\frac{\partial p}{\partial p} \right)_{s, Y_1, Y_2, \dots, Y_{N-1}} = RT \left(1 + \frac{R}{c_v}\right) \quad (2.32)$$

Eq. (2.26) now follows immediately from Eqs. (2.25), (2.32), (2.14), and (2.20). QED.

2.2 Governing Equations

We assume that the N gas species considered here share a common flow velocity u . Let the total specific energy

$$E \stackrel{\text{def}}{=} e + \frac{u^2}{2} \quad (2.33)$$

Let $\dot{\omega}_i, i = 1, 2, \dots, N$, be the net mass of species i generated per unit time and per unit volume from all chemical reactions involved. Because mass is conserved during any chemical reaction, we have

$$\sum_{i=1}^N \dot{\omega}_i = 0 \quad (2.34)$$

Furthermore, let

$$u_1^{def} = \rho, u_2^{def} = \rho u, u_3^{def} = \rho E, u_{3+i}^{def} = \rho_i \quad (i = 1, 2, \dots, N) \quad (2.35)$$

$$f_1^{def} = \rho u, f_2^{def} = \rho u^2 + p, f_3^{def} = u(\rho E + p), f_{3+i}^{def} = u \rho_i \quad (i = 1, 2, \dots, N) \quad (2.36)$$

$$b_1^{def} = 0, b_2^{def} = 0, b_3^{def} = 0, b_{3+i}^{def} = \dot{\omega}_i \quad (i = 1, 2, \dots, N) \quad (2.37)$$

Then the 1D unsteady Euler equations for a chemically reacting mixture of N thermally perfect gas species in thermal equilibrium with each other can be written as

$$\frac{\partial u_m}{\partial t} + \frac{\partial f_m}{\partial x} = b_m \quad (m = 1, 2, \dots, N + 2) \quad (2.38a)$$

Note that: (a) In Eq. (2.38a), the equations with $m = 1, 2, 3$, respectively, represent the mass, momentum, and energy conservation relations for the mixture. On the other hand, those with $m = 4, 5, \dots, N + 2$, respectively, represent the mass conservation relations for species $i = 1, 2, \dots, N - 1$. Moreover, with the aid of Eqs. (2.4) and (2.34), the mass conservation relation for species N can be derived from the mass conservation relations for the mixture and species $i = 1, 2, \dots, N - 1$. As such the former (i.e., the equation with $m = N + 3$) becomes redundant and therefore is not included in Eq. (2.38a). (b) Let \vec{u} , \vec{f} , and \vec{b} , respectively, be the column matrices formed by u_m , f_m , and b_m , $m = 1, 2, \dots, N + 2$. Then the matrix form of Eq. (2.38a) is

$$\frac{\partial \vec{u}}{\partial t} + \frac{\partial \vec{f}}{\partial x} = \vec{b} \quad (2.38b)$$

(c) By using Eqs. (2.35) and (2.36), it can be shown that

$$f_1 = u_2, f_2 = \frac{(u_2)^2}{u_1} + p, f_3 = \frac{u_2}{u_1}(u_3 + p), f_{3+i} = \frac{u_2 u_{3+i}}{u_1} \quad (i = 1, 2, \dots, N - 1) \quad (2.39)$$

i.e., each f_m , $m = 1, 2, \dots, N+2$ can be expressed explicitly in terms of p and u_m ,
 $m = 1, 2, \dots, N+2$. Moreover, by using Eq. (2.18) and the relations

$$e = \frac{u_3}{u_1} - \frac{1}{2} \left(\frac{u_2}{u_1} \right)^2, \quad \rho = u_1, \quad \rho_i = u_{3+i} \quad (i = 1, 2, \dots, N-1) \quad (2.40)$$

which follow from Eqs. (2.33) and (2.35), one concludes that implicitly p is also a function of u_m , $m = 1, 2, \dots, N+2$. Thus implicitly f_m , $m = 1, 2, 3, \dots, N+2$, are functions of u_m , $m = 1, 2, \dots, N+2$.

(d) It will be shown in Sec. 2.4 that, implicitly $\dot{\omega}_i$, $i = 1, 2, 3, \dots, N-1$ are also functions of u_m , $m = 1, 2, \dots, N+2$.

From the above discussions, one concludes that Eq. (2.38a) represents a system of $N+2$ independent equations for $N+2$ unknowns of u_m , $m = 1, 2, \dots, N+2$.

2.3. Jacobian Matrix of Flux Functions

With the aid of Eqs. (2.18), (2.20)–(2.22), and (2.40), an application of the chain rule leads to

$$\frac{\partial p}{\partial u_1} = p_\rho + \left(\frac{u^2}{2} - e \right) \frac{p_e}{\rho}, \quad \frac{\partial p}{\partial u_2} = -\frac{u p_e}{\rho}, \quad \frac{\partial p}{\partial u_3} = \frac{p_e}{\rho}, \quad \frac{\partial p}{\partial u_{3+i}} = p_{\rho_i} \quad (i = 1, 2, \dots, N-1) \quad (2.41)$$

Hereafter, without using explicit notations, let it be understood that a partial derivative with respect to any u_m will always be evaluated assuming that, except u_m , all other independent variables in the set $\{u_1, u_2, \dots, u_{N+2}\}$ are held constant.

Let A be the $(N+2) \times (N+2)$ Jacobian matrix with the element on the m th row and the ℓ th column being $\partial f_m / \partial u_\ell$. Then Eqs. (2.39) and (2.41) imply that

$$A = \begin{pmatrix} 0 & 1 & 0 & 0 & 0 & \dots & 0 \\ p_\rho - \frac{e}{\rho} p_e - u^2(1 - \frac{p_e}{2\rho}) & u(2 - \frac{p_e}{\rho}) & \frac{p_e}{\rho} & p_{\rho_1} & p_{\rho_2} & \dots & p_{\rho_{N-1}} \\ u(p_\rho - H + \frac{u^2}{2\rho} p_e - \frac{e}{\rho} p_e) & H - \frac{u^2}{\rho} p_e & u(1 + \frac{p_e}{\rho}) & up_{\rho_1} & up_{\rho_2} & \dots & up_{\rho_{N-1}} \\ -\frac{u}{\rho} \rho_1 & \frac{\rho_1}{\rho} & 0 & u & 0 & \dots & 0 \\ -\frac{u}{\rho} \rho_2 & \frac{\rho_2}{\rho} & 0 & 0 & u & \dots & 0 \\ \vdots & \vdots & \vdots & \vdots & \vdots & \ddots & \vdots \\ -\frac{u}{\rho} \rho_{N-1} & \frac{\rho_{N-1}}{\rho} & 0 & 0 & 0 & \dots & u \end{pmatrix} \quad (2.42)$$

where

$$H \stackrel{def}{=} E + p/\rho = \sum_{i=1}^N Y_i (e_i + \frac{u^2}{2} + \frac{p_i}{\rho_i}) \quad (2.43)$$

is the total enthalpy of the gas mixture. Note that: (i) the validity of the last equality sign in Eq. (2.43) can be established using Eqs. (2.2), (2.3), (2.5), (2.7), and (2.33); and (ii) because $\partial f_m / \partial x = \sum_{t=1}^{N+2} (\partial f_m / \partial u_t) (\partial u_t / \partial x)$, Eq. (2.38b) is equivalent to

$$\frac{\partial \vec{u}}{\partial t} + A \frac{\partial \vec{u}}{\partial x} = \vec{b} \quad (2.44)$$

Furthermore, by using Eqs. (2.23), (2.33), (2.35), (2.36), (2.42), and (2.43), it can be shown that

$$\begin{pmatrix} \rho u \\ \rho u^2 + \rho p_\rho + \sum_{i=1}^{N-1} \rho_i p_{\rho_i} \\ \rho u E + u(\rho p_\rho + \sum_{i=1}^{N-1} \rho_i p_{\rho_i}) \\ u \rho_1 \\ u \rho_2 \\ \vdots \\ u \rho_{N-1} \end{pmatrix} = \begin{pmatrix} \rho u \\ \rho u^2 + p \\ u(\rho E + p) \\ u \rho_1 \\ u \rho_2 \\ \vdots \\ u \rho_{N-1} \end{pmatrix} = \vec{f} \quad (2.45)$$

According to a theorem given on pp.11-12 in [22], Eq. (2.45) implies that each flux function f_m , $m = 1, 2, \dots, N+2$, is a homogeneous function of degree 1 in the variables u_1, u_2, \dots, u_{N+2} .

For a reason that will become clear soon, next we will introduce a set of new independent variables u_m , $m = 1, 2, \dots, N+2$, i.e.,

$$\stackrel{def}{u_1} = \rho, \quad \stackrel{def}{u_2} = u, \quad \stackrel{def}{u_3} = e, \quad \stackrel{def}{u_{3+i}} = Y_i, \quad (i = 1, 2, \dots, N-1) \quad (2.46)$$

By using Eqs. (2.3), (2.33), (2.35), and (2.46), it can be shown that

$$\underline{u}_1 = u_1, \quad \underline{u}_2 = \frac{u_2}{u_1}, \quad \underline{u}_3 = \frac{u_3}{u_1} - \frac{1}{2} \left(\frac{u_2}{u_1} \right)^2, \quad \underline{u}_{3+i} = \frac{u_{3+i}}{u_1} \quad (i = 1, 2, \dots, N-1) \quad (2.47)$$

and

$$u_1 = \underline{u}_1, \quad u_2 = \underline{u}_1 \underline{u}_2, \quad u_3 = \underline{u}_1 \underline{u}_3 + \frac{\underline{u}_1 (\underline{u}_2)^2}{2}, \quad u_{3+i} = \underline{u}_1 \underline{u}_{3+i} \quad (i = 1, 2, \dots, N-1) \quad (2.48)$$

Let T be the $(N+2) \times (N+2)$ matrix with the element on the m th row and the ℓ th column being $\partial \underline{u}_m / \partial u_\ell$. Then, by the chain rule, it can be shown that T^{-1} (i.e., the inverse of T) is the $(N+2) \times (N+2)$ matrix with the element on the m th row and the ℓ th column being $\partial u_m / \partial \underline{u}_\ell$.

By using Eqs. (2.47) and (2.48), one has

$$T = \begin{pmatrix} 1 & 0 & 0 & 0 & 0 & \dots & 0 \\ -\frac{u}{\rho} & \frac{1}{\rho} & 0 & 0 & 0 & \dots & 0 \\ \frac{u^2 - E}{\rho} & -\frac{u}{\rho} & \frac{1}{\rho} & 0 & 0 & \dots & 0 \\ -\frac{\rho_1}{\rho^2} & 0 & 0 & \frac{1}{\rho} & 0 & \dots & 0 \\ -\frac{\rho_2}{\rho^2} & 0 & 0 & 0 & \frac{1}{\rho} & \dots & 0 \\ \vdots & \vdots & \vdots & \vdots & \vdots & \ddots & \vdots \\ -\frac{\rho_{N-1}}{\rho^2} & 0 & 0 & 0 & 0 & \dots & \frac{1}{\rho} \end{pmatrix},$$

$$T^{-1} = \begin{pmatrix} 1 & 0 & 0 & 0 & 0 & \dots & 0 \\ u & \rho & 0 & 0 & 0 & \dots & 0 \\ E & \rho u & \rho & 0 & 0 & \dots & 0 \\ \frac{\rho_1}{\rho} & 0 & 0 & \rho & 0 & \dots & 0 \\ \frac{\rho_2}{\rho} & 0 & 0 & 0 & \rho & \dots & 0 \\ \vdots & \vdots & \vdots & \vdots & \vdots & \ddots & \vdots \\ \frac{\rho_{N-1}}{\rho} & 0 & 0 & 0 & 0 & \dots & \rho \end{pmatrix} \quad (2.49)$$

Next, note that

$$\frac{\partial \rho}{\partial t} + u \frac{\partial \rho}{\partial x} + \rho \frac{\partial u}{\partial x} = 0 \quad (2.50)$$

$$\frac{\partial u}{\partial t} + u \frac{\partial u}{\partial x} + \frac{1}{\rho} \frac{\partial p}{\partial x} = 0 \quad (2.51)$$

$$\frac{\partial e}{\partial t} + \frac{p}{\rho} \frac{\partial u}{\partial x} + u \frac{\partial e}{\partial x} = 0 \quad (2.52)$$

and

$$\frac{\partial \rho_i}{\partial t} + u \frac{\partial \rho_i}{\partial x} + \rho_i \frac{\partial u}{\partial x} = \dot{\omega}_i \quad (i=1,2,\dots,N-1) \quad (2.53)$$

form an equivalent non-conservative form of Eq. (2.38a). By using the relations (i)

$$\frac{\partial p}{\partial x} = p_\rho \frac{\partial \rho}{\partial x} + p_e \frac{\partial e}{\partial x} + \sum_{i=1}^{N-1} p_{\rho_i} \frac{\partial \rho_i}{\partial x} \quad (2.54)$$

(ii)

$$\frac{\partial \rho_i}{\partial x} = \frac{\partial(\rho Y_i)}{\partial x} = \rho \frac{\partial Y_i}{\partial x} + Y_i \frac{\partial \rho}{\partial x} \quad (i=1,2,\dots,N-1) \quad (2.55)$$

(iii) $Y_i / \rho = \rho_i / (\rho^2)$, $i = 1,2,\dots,N-1$, and (iv) Eq. (2.23), Eq. (2.51) can be recast as

$$\frac{\partial u}{\partial t} + \frac{p}{\rho^2} \frac{\partial \rho}{\partial x} + u \frac{\partial u}{\partial x} + \frac{p_e}{\rho} \frac{\partial e}{\partial x} + \sum_{i=1}^{N-1} p_{\rho_i} \frac{\partial Y_i}{\partial x} = 0 \quad (2.51a)$$

Furthermore, with the aid of Eq. (2.50) and the fact that $\rho_i = \rho Y_i$, $i = 1,2,\dots,N-1$, Eq. (2.53) can be simplified as

$$\frac{\partial Y_i}{\partial t} + u \frac{\partial Y_i}{\partial x} = \frac{\dot{\omega}_i}{\rho}, \quad (i=1,2,\dots,N-1) \quad (2.53a)$$

From the above discussions, one concludes that the system of equations represented by Eq. (2.38a) is equivalent to the system of equations formed by Eqs. (2.50), (2.51a), (2.52), and (2.53a). With the aid of Eqs. (2.46) and (2.49), and

$$\underline{A} \stackrel{def}{=} \begin{pmatrix} u & \rho & 0 & 0 & 0 & \dots & 0 \\ \frac{p}{\rho^2} & u & \frac{p_e}{\rho} & p_{\rho_1} & p_{\rho_2} & \dots & p_{\rho_{N-1}} \\ 0 & \frac{p}{\rho} & u & 0 & 0 & \dots & 0 \\ 0 & 0 & 0 & u & 0 & \dots & 0 \\ 0 & 0 & 0 & 0 & u & \dots & 0 \\ \vdots & \vdots & \vdots & \vdots & \vdots & \ddots & \vdots \\ 0 & 0 & 0 & 0 & 0 & \dots & u \end{pmatrix} \quad (2.56)$$

The latter system can be expressed as

$$\frac{\partial \underline{u}}{\partial t} + \underline{A} \frac{\partial \underline{u}}{\partial x} = T \bar{b} \quad (2.57)$$

where \underline{u} is the column matrix formed by u_m , $m=1,2,\dots,N+2$.

Next, by the chain rule, one has $\partial \underline{u}_m / \partial t = \sum_{t=1}^{N+2} (\partial \underline{u}_m / \partial u_t) (\partial u_t / \partial x)$. Thus, by the definition of T , one concludes that $\partial \underline{u} / \partial t = T \partial u / \partial t$. Similarly, one has $\partial \underline{u} / \partial x = T \partial u / \partial x$. Thus, by multiplying Eq. (2.57) from the left with T^{-1} , one concludes that

$$\frac{\partial U}{\partial t} + T^{-1} \underline{A} T \frac{\partial U}{\partial x} = \bar{b} \quad (2.58)$$

Because Eq. (2.58) is equivalent to Eq. (2.44), one concludes that $(A - T^{-1} \underline{A} T) \partial U / \partial x \equiv 0$. The last identity is valid if and only if

$$A \equiv T^{-1} \underline{A} T \quad (2.59)$$

In fact, with the aid of Eq. (2.23), Eq. (2.59) can also be established directly using Eqs. (2.42), (2.49) and (2.56).

According to Eq. (2.59), A and \underline{A} are related by a similarity transformation. Thus they have identical eigenvalues, counting multiplicity [22]. However, compared with A , \underline{A} has a

simpler form. In particular, the $(N+2) \times (N+2)$ matrix \underline{A} has the special property that the only possible non-zero element on each of its lowest $N-1$ rows is the diagonal element u . As will be shown shortly, because of this special property, the eigenvalues of \underline{A} (and therefore those of A) can be evaluated in a straightforward fashion.

To proceed, let M be any $K \times K$ matrix with $m_{i,j}$ being its element at the i th row and j th column. Let $\det M$ be the determinant of M . Then, according to a basic theory of determinant, for any given $i = 1, 2, \dots, K$,

$$\det M = \sum_{j=1}^K m_{i,j} \times (\text{cofactor of } m_{i,j}) \quad (2.60)$$

Furthermore, let (i) I_K denote the $K \times K$ identity matrix for any integer $K > 0$; and (ii) λ be a scalar. Then the special property of \underline{A} referred to in the last paragraph coupled with a repeated application of Eq. (2.60) implies that

$$\det(\underline{A} - \lambda I_{N+2}) = (u - \lambda)^{N-1} \times \det(\underline{A}_3 - \lambda I_3) \quad (2.61)$$

where \underline{A}_3 is the 3×3 submatrix located at the top-left corner of \underline{A} , i.e.,

$$\underline{A}_3 \stackrel{\text{def}}{=} \begin{pmatrix} u & \rho & 0 \\ \frac{p}{\rho^2} & u & \frac{p_e}{\rho} \\ 0 & \frac{p}{\rho} & u \end{pmatrix} \quad (2.62)$$

Because the eigenvalues of \underline{A} (and thus those of A) are the roots of $\det(\underline{A} - \lambda I_{N+2}) = 0$, by combining (i) Eq. (2.61), (ii)

$$\det(\underline{A}_3 - \lambda I_3) = (u - \lambda) \left[(u - \lambda)^2 - \frac{p}{\rho} \left(1 + \frac{p_e}{\rho} \right) \right] \quad (2.63)$$

and (iii) Eq. (2.26), one concludes that \underline{A} (and thus A) has three distinct eigenvalues, i.e., $u + a_f$, $u - a_f$, and u , with u being an eigenvalue of multiplicity N .

Even though they are not needed in the CE/SE development, for completeness, the eigenvectors of the matrices \underline{A} and A will be constructed and given explicitly in the remainder of this subsection.

Let M' denote the transpose of any matrix M . Let $\vec{\phi} = (\phi_1, \phi_2, \dots, \phi_{N+2})$ be an eigenvector of \underline{A} with the eigenvalue $u + a_f$, i.e., it is a nontrivial solution to

$$\left[\underline{A} - (u + a_f) I_{N+2} \right] \vec{\phi} = 0 \quad (2.64)$$

According to Eq. (2.56), Eq. (2.64) is equivalent to

$$-a_f \phi_1 + \rho \phi_2 = 0 \quad (2.65a)$$

$$\frac{P}{\rho^2} \phi_1 - a_f \phi_2 + \frac{P_e}{\rho} \phi_3 + \sum_{\ell=1}^{N-1} P_{\rho_\ell} \phi_{\ell+3} = 0 \quad (2.65b)$$

$$\frac{P}{\rho} \phi_2 - a_f \phi_3 = 0 \quad (2.65c)$$

and

$$a_f \phi_\ell = 0 \quad \ell=4, 5, \dots, N+2 \quad (2.65d)$$

Because $a_f > 0$ and $\rho > 0$, Eqs. (2.65a), (2.65c), and (2.65d) imply that

$$\phi_1 = \frac{\rho}{a_f} \phi_2; \quad \phi_3 = \frac{P}{\rho a_f} \phi_2; \quad \text{and } \phi_\ell = 0 \text{ for } \ell=4, 5, \dots, N+2 \quad (2.66)$$

Moreover, with the aid of Eq. (2.26), it can be shown that Eq. (2.65b) is automatically satisfied if Eq. (2.66) is assumed. As such, Eq. (2.64) is equivalent to Eq. (2.66), i.e., any nonzero $\vec{\phi}$ that satisfies Eq. (2.66) is an eigenvector of \underline{A} with the eigenvalue $u + a_f$. Let $\phi_2 = 1$. Then Eq. (2.66) implies that the $(N+2) \times 1$ column matrix

$$\vec{\phi}^{(1)} \stackrel{\text{def}}{=} \left(\frac{\rho}{a_f}, 1, \frac{P}{\rho a_f}, 0, 0, \dots, 0 \right)^T \quad (2.67)$$

is an eigenvector of \underline{A} with the eigenvalue $u + a_f$, i.e.,

$$\left[\underline{A} - (u + a_f) I_{N+2} \right] \vec{\phi}^{(1)} = 0 \quad (2.68)$$

Similarly, it can be shown that the $(N+2) \times 1$ column matrix

$$\vec{\phi}^{(2)} \stackrel{\text{def}}{=} \left(-\frac{\rho}{a_f}, 1, -\frac{P}{\rho a_f}, 0, 0, \dots, 0 \right)^T \quad (2.69)$$

is an eigenvector of \underline{A} with the eigenvalue $u - a_f$, i.e.,

$$[\underline{A} - (u - a_f)I_{N+2}] \vec{\phi}^{(2)} = 0 \quad (2.70)$$

Next, let $\vec{\phi} = (\phi_1, \phi_2, \dots, \phi_{N+2})$ be an eigenvector of \underline{A} with the eigenvalue u , i.e., it is a nontrivial solution to

$$[\underline{A} - uI_{N+2}] \vec{\phi} = 0 \quad (2.71)$$

According to Eq. (2.56), Eq. (2.71) is equivalent to

$$\rho \phi_2 = 0 \quad (2.72a)$$

$$\frac{P}{\rho^2} \phi_1 + \frac{P_e}{\rho} \phi_3 + \sum_{\ell=1}^{N-1} p_{\rho_\ell} \phi_{\ell+3} = 0 \quad (2.72b)$$

and

$$\frac{P}{\rho} \phi_2 = 0 \quad (2.72c)$$

Because $\rho > 0$ and $P > 0$, Eq. (2.72a) and (2.72c) reduce to

$$\phi_2 = 0 \quad (2.73)$$

Thus Eq. (2.71) represents two independent conditions (i.e., Eqs. (2.72b) and (2.73)) for $N+2$ variables. As such it can have only N linearly independent solutions. Let

$$\vec{\phi}^{(m)} \stackrel{\text{def}}{=} (\phi_1^{(m)}, \phi_1^{(m)}, \dots, \phi_{N+2}^{(m)})^t, \quad m = 3, 4, \dots, N+2 \quad (2.74)$$

where (i)

$$\phi_1^{(3)} = -\frac{\rho P_e}{P}; \text{ and } \phi_\ell^{(3)} = \delta_\ell^3 \text{ for } \ell = 2, 3, \dots, N+2 \quad (2.75a)$$

and (ii) for any $m = 4, 5, \dots, N+2$,

$$\phi_1^{(m)} = -\frac{\rho^2 P_{\rho_{m-3}}}{P}; \text{ and } \phi_\ell^{(m)} = \delta_\ell^m \text{ for } \ell = 2, 3, \dots, N+2 \quad (2.75b)$$

with δ_ℓ^m (any m and ℓ) being the Kronecher delta symbol. Then it can be shown that $\vec{\phi}^{(m)}, m = 3, 4, \dots, N+2$, are eigenvectors of \underline{A} with the eigenvalue u , i.e.,

$$[\underline{A} - uI_{N+2}] \vec{\phi}^{(m)} = 0, \quad m = 3, 4, \dots, N+2 \quad (2.76)$$

As will be shown, these eigenvectors are also linearly independent.

Let Φ be the $(N+2) \times (N+2)$ matrix formed using the column matrix $\vec{\phi}^{(m)}$, $m=1,2,\dots,N+2$, i.e., for any ℓ , $m=1,2,\dots,N+2$, the element on the ℓ th row and m th column of Φ is the ℓ th element of the column matrix $\vec{\phi}^{(m)}$. Then (i)

$$\Phi = \begin{pmatrix} \frac{\rho}{a_f} & -\frac{\rho}{a_f} & -\frac{\rho p_e}{p} & -\frac{\rho^2 p_{\rho_1}}{p} & -\frac{\rho^2 p_{\rho_2}}{p} & \dots & -\frac{\rho^2 p_{\rho_{N-1}}}{p} \\ 1 & 1 & 0 & 0 & 0 & \dots & 0 \\ \frac{p}{\rho a_f} & -\frac{p}{\rho a_f} & 1 & 0 & 0 & \dots & 0 \\ 0 & 0 & 0 & 1 & 0 & \dots & 0 \\ 0 & 0 & 0 & 0 & 1 & \dots & 0 \\ \vdots & \vdots & \vdots & \vdots & \vdots & \ddots & \vdots \\ 0 & 0 & 0 & 0 & 0 & \dots & 1 \end{pmatrix} \quad (2.77)$$

(ii) with the aid of Eqs. (2.4), (2.20) and (2.26), one has

$$\det \Phi \equiv 2 \left(\frac{\rho + p_e}{a_f} \right) > 0 \quad (2.78)$$

i.e., Φ is nonsingular; and (iii) Eqs. (2.68), (2.70), and (2.76) are equivalent to

$$\underline{A}\Phi = \Phi\Lambda \quad (2.79)$$

where Λ is the $(N+2) \times (N+2)$ diagonal matrix defined by

$$\Lambda \stackrel{def}{=} \begin{pmatrix} u+a_f & 0 & 0 & 0 & \dots & 0 \\ 0 & u-a_f & 0 & 0 & \dots & 0 \\ 0 & 0 & u & 0 & \dots & 0 \\ 0 & 0 & 0 & u & \dots & 0 \\ \vdots & \vdots & \vdots & \vdots & \ddots & \vdots \\ 0 & 0 & 0 & 0 & \dots & u \end{pmatrix} \quad (2.80)$$

Note that, because Φ is formed using the eigenvectors $\vec{\phi}^{(m)}$, $m=1,2,\dots,N+2$, nonsingularity of Φ implies that these eigenvectors are linearly independent.

For any square matrix M and any eigenvalue a of M , let $ES(M:a)$ denote the eigenspace of M with the eigenvalue a . Then because (i) $\vec{\phi}^{(m)}$, $m=1,2,\dots,N+2$, are linear independent, and (ii) the multiplicities of the eigenvalues $u+a_f$, $u-a_f$, and u are 1, 1, and N ,

respectively, one concludes that (i) $\{\vec{\phi}^{(1)}\}$ forms a basis of $ES(\underline{A}: a + u_f)$; (ii) $\{\vec{\phi}^{(2)}\}$ forms a basis of $ES(\underline{A}: a - u_f)$; and (iii) $\{\vec{\phi}^{(3)}, \vec{\phi}^{(4)}, \dots, \vec{\phi}^{(N+2)}\}$ forms a basis of $ES(\underline{A}: a + u)$. In other words, (i) a column matrix is an eigenvector of \underline{A} with the eigenvalue $u + a_f$ if and only it can be expressed as $\beta \vec{\phi}^{(1)}$ with β being a nonzero scalar; (ii) a column matrix is an eigenvector of \underline{A} with the eigenvalue $u - a_f$ if and only it can be expressed as $\beta \vec{\phi}^{(2)}$ with β being a nonzero scalar; and (iii) a column matrix is an eigenvector of \underline{A} with the eigenvalue u if and only it can be expressed as a linear combination of $\vec{\phi}^{(m)}$, $m = 3, 4, \dots, N + 2$, where not all combination coefficients vanish.

Next, by using the relation $\underline{A} = TAT^{-1}$ which follows from Eq. (2.59), Eq. (2.79) implies that

$$A\Psi = \Psi\Lambda \quad (2.81)$$

where

$$\Psi \stackrel{def}{=} T^{-1}\Phi \quad (2.82)$$

Because $\det(T^{-1}) = \rho^{N+1} > 0$ (see Eq. (2.49)), Eqs. (2.78) and (2.82) implies that

$$\det \Psi = \det(T^{-1}) \cdot \det \Phi > 0 \quad (2.83)$$

i.e., Ψ is nonsingular.

Let

$$\bar{\psi}^{(1)} \stackrel{def}{=} \left(\frac{\rho}{a_f}, \frac{\rho}{a_f}(u + a_f), \frac{\rho}{a_f}(H + ua_f), \frac{\rho_1}{a_f}, \frac{\rho_2}{a_f}, \dots, \frac{\rho_{N-1}}{a_f} \right)^t \quad (2.84a)$$

$$\bar{\psi}^{(2)} \stackrel{def}{=} \left(\frac{\rho}{a_f}, \frac{\rho}{a_f}(u - a_f), \frac{\rho}{a_f}(H - ua_f), \frac{\rho_1}{a_f}, \frac{\rho_2}{a_f}, \dots, \frac{\rho_{N-1}}{a_f} \right)^t \quad (2.84b)$$

$$\bar{\psi}^{(3)} \stackrel{def}{=} \left(\frac{\rho p_e}{p}, \frac{\rho p_e u}{p}, \frac{\rho p_e}{p} \left(H - \frac{\rho}{p_e} (a_f)^2 \right), \frac{\rho_1 p_e}{p}, \frac{\rho_2 p_e}{p}, \dots, \frac{\rho_{N-1} p_e}{p} \right)^t \quad (2.84c)$$

and, for $m = 4, 5, \dots, N + 2$,

$$\begin{aligned} \bar{\psi}^{(m)} \stackrel{\text{def}}{=} & \left(\frac{\rho^2 p_{\rho_{m-3}}}{p}, \frac{\rho^2 p_{\rho_{m-3}} u}{p}, \frac{\rho^2 p_{\rho_{m-3}} E}{p}, \frac{\rho \rho_1 p_{\rho_{m-3}}}{p} - \rho \delta_1^{m-3}, \frac{\rho \rho_2 p_{\rho_{m-3}}}{p} - \rho \delta_2^{m-3}, \right. \\ & \left. \dots, \frac{\rho \rho_{N-1} p_{\rho_{m-3}}}{p} - \rho \delta_{N-1}^{m-3} \right)^t, \quad m = 4, 5, \dots, N+2 \end{aligned} \quad (2.84d)$$

Then, with the aid of Eqs. (2.14), (2.20), (2.26), (2.43), (2.49), (2.77) and (2.82), it can be shown that the nonsingular matrix Ψ is formed using the column matrices $\bar{\psi}^{(m)}$, $m = 1, 2, \dots, N+2$. As such, (i) these $N+2$ column matrices are linearly independent; and (ii) Eq. (2.81) is equivalent to

$$\left[A - (u + a_f) I_{N+2} \right] \bar{\psi}^{(1)} = 0 \quad (2.85a)$$

$$\left[A - (u - a_f) I_{N+2} \right] \bar{\psi}^{(2)} = 0 \quad (2.85b)$$

and

$$\left[A - u I_{N+2} \right] \bar{\psi}^{(m)} = 0, \quad m = 3, 4, \dots, N+2 \quad (2.85c)$$

Thus (i) $\{\bar{\psi}^{(1)}\}$ forms a basis of $ES(\underline{A} : a + u_f)$; (ii) $\{\bar{\psi}^{(2)}\}$ forms a basis of $ES(\underline{A} : a - u_f)$; and (iii) $\{\bar{\psi}^{(3)}, \bar{\psi}^{(4)}, \dots, \bar{\psi}^{(N+2)}\}$ forms a basis of $ES(\underline{A} : a + u)$. In the following, bases with simpler structure will be constructed.

As a preliminary, note that Eqs. (2.26) and (2.43) implies that

$$H - E - \frac{\rho}{p_e} (a_f)^2 = \frac{p}{\rho} - \frac{\rho}{p_e} \frac{p}{\rho} \left(1 + \frac{p_e}{\rho} \right) = -\frac{p}{p_e} \quad (2.86)$$

Then, (i) Eqs. (2.84a), (2.84b), and (2.84c) imply that

$$\bar{\theta}^{(1)} \stackrel{\text{def}}{=} \frac{a_f}{\rho} \bar{\psi}^{(1)} = \left(1, u + a_f, H + u a_f, \frac{\rho_1}{\rho}, \frac{\rho_2}{\rho}, \dots, \frac{\rho_{N-1}}{\rho} \right)^t \quad (2.87a)$$

$$\bar{\theta}^{(2)} \stackrel{\text{def}}{=} \frac{a_f}{\rho} \bar{\psi}^{(2)} = \left(1, u - a_f, H - u a_f, \frac{\rho_1}{\rho}, \frac{\rho_2}{\rho}, \dots, \frac{\rho_{N-1}}{\rho} \right)^t \quad (2.87b)$$

$$\bar{\theta}^{(3)} \stackrel{\text{def}}{=} \frac{p}{\rho p_e} \bar{\psi}^{(3)} = \left(1, u, H - \frac{\rho (a_f)^2}{p_e}, \frac{\rho_1}{\rho}, \frac{\rho_2}{\rho}, \dots, \frac{\rho_{N-1}}{\rho} \right)^t \quad (2.87c)$$

and

$$\bar{\theta}^{(m)} \stackrel{\text{def}}{=} \bar{\psi}^{(m)} - \frac{\rho p_{\rho_{m-3}}}{p_e} \bar{\psi}^{(3)} = \left(0, 0, -\frac{\rho^2 p_{\rho_{m-3}}}{p_e}, \rho \delta_1^{m-3}, \rho \delta_2^{m-3}, \dots, \rho \delta_{N-1}^{m-3} \right)^t \quad (2.87d)$$

$$m = 4, 5, \dots, N+2$$

Let Θ be the matrix formed using the column matrices $\bar{\theta}^{(m)}$, $m = 1, 2, \dots, N+2$, i.e.,

$$\Theta = \begin{pmatrix} 1 & 1 & 1 & 0 & 0 & \dots & 0 \\ u + a_f & u - a_f & u & 0 & 0 & \dots & 0 \\ H + ua_f & H - ua_f & H - \frac{\rho}{p_e} (a_f)^2 & -\frac{\rho^2 p_{\rho_1}}{p_e} & -\frac{\rho^2 p_{\rho_2}}{p_e} & \dots & -\frac{\rho^2 p_{\rho_{N-1}}}{p_e} \\ \frac{\rho_1}{\rho} & \frac{\rho_1}{\rho} & \frac{\rho_1}{\rho} & \rho & 0 & \dots & 0 \\ \frac{\rho_2}{\rho} & \frac{\rho_2}{\rho} & \frac{\rho_2}{\rho} & 0 & \rho & \dots & 0 \\ \vdots & \vdots & \vdots & \vdots & \vdots & \ddots & \vdots \\ \frac{\rho_{N-1}}{\rho} & \frac{\rho_{N-1}}{\rho} & \frac{\rho_{N-1}}{\rho} & 0 & 0 & \dots & \rho \end{pmatrix} \quad (2.88)$$

Then, with the aid of the fact that Ψ is the matrix formed using $\bar{\psi}^{(m)}$, $m = 1, 2, \dots, N+2$, Eqs. (2.87a)–(2.87d) imply that

$$\Theta = \Psi Q \quad (2.89)$$

where

$$Q \stackrel{\text{def}}{=} \begin{pmatrix} \frac{a_f}{\rho} & 0 & 0 & 0 & 0 & \dots & 0 \\ 0 & -\frac{a_f}{\rho} & 0 & 0 & 0 & \dots & 0 \\ 0 & 0 & -\frac{p}{\rho p_e} & -\frac{\rho p_{\rho_1}}{p_e} & -\frac{\rho p_{\rho_2}}{p_e} & \dots & -\frac{\rho p_{\rho_{N-1}}}{p_e} \\ 0 & 0 & 0 & 1 & 0 & \dots & 0 \\ 0 & 0 & 0 & 0 & 1 & \dots & 0 \\ \vdots & \vdots & \vdots & \vdots & \vdots & \ddots & \vdots \\ 0 & 0 & 0 & 0 & 0 & \dots & 1 \end{pmatrix} \quad (2.90)$$

Because $\det Q = p(a_f)^2 / (\rho^3 p_e) > 0$, Eqs. (2.89) and (2.83) implies that

$$\det \Theta = \det \Psi \cdot \det Q > 0 \quad (2.91)$$

i.e., Θ is nonsingular. In turn, this implies that $\bar{\theta}^{(m)}, m = 1, 2, \dots, N + 2$, are linearly independent. Moreover, because $\Lambda Q \doteq Q\Lambda$, Eqs. (2.81) and (2.89) implies that

$$A\Theta = \Theta\Lambda \quad (2.92)$$

i.e., Eqs. (2.85a)–(2.85c) remain valid if, for each $m = 1, 2, \dots, N + 2$, $\psi^{(m)}$ is replaced by $\bar{\theta}^{(m)}$. As such, one concludes that (i) $\{\bar{\theta}^{(1)}\}$ forms a basis of $ES(\underline{A}: a + u_f)$; (ii) $\{\bar{\theta}^{(2)}\}$ forms a basis of $ES(\underline{A}: a - u_f)$; and (iii) $\{\bar{\theta}^{(3)}, \bar{\theta}^{(4)}, \dots, \bar{\theta}^{(N+2)}\}$ forms a basis of $ES(\underline{A}: a + u)$.

Note that, for the special case $N = 5$, (i) $[\rho/\sqrt{2}a_f]\bar{\theta}^{(1)}, [\rho/\sqrt{2}a_f]\bar{\theta}^{(2)}$, and $\bar{\theta}^{(3)}$, respectively, reduce to the second, the third, and the first column matrices contained in the matrix S ; and (ii) for each $m = 4, 5, 6, 7$, $\bar{\theta}^{(m)}$ reduces to the m th column matrix contained in S . Note that the symbols $\rho_1, \rho_2, \dots, \rho_{N-1}$ and a_f used here, respectively, are replaced by C_1, C_2, \dots, C_{N-1} and a .

2.4 Evaluation of Thermodynamic/Chemical Parameters

Let (i) h_i and c_{pi} be the specific enthalpy and the specific heat at constant pressure of species i , respectively; and (ii)

$$\hat{h}_i \stackrel{\text{def}}{=} M_i h_i, \quad \hat{s}_i \stackrel{\text{def}}{=} M_i s_i, \quad \hat{c}_{pi} \stackrel{\text{def}}{=} M_i c_{pi} \quad (2.93)$$

Because M_i and s_i are the molecular weight and the specific entropy of species i , respectively, Eq. (2.93) implies that \hat{h}_i, \hat{s}_i , and \hat{c}_{pi} are the molar specific enthalpy, the molar specific entropy, and the molar specific heat at constant pressure of species i , respectively.

Because the gas mixture is thermally perfect (which is a good approximation as long as each p_i is in the order of 1 atm or less), for each species i , $\hat{h}_i = \hat{h}_i(T)$ and $\hat{c}_{pi} = \hat{c}_{pi}(T)$. Furthermore, in the current study, each $\hat{c}_{pi}(T)$ is approximated using a polynomial of T , i.e.,

$$\frac{\hat{c}_{pi}(T)}{R_u} = \sum_{t=0}^4 a_{it} T^t \quad (2.94)$$

where the coefficients a_{ij} can be found in NASA CEA program data base. By using Eq. (2.94) and the relation

$$\hat{h}_i(T) = \int_{T_{ref}}^T \hat{c}_{pi}(T') dT' + \hat{h}_{fi} \quad (2.95)$$

where \hat{h}_{fi} is the molar heat of formation for species i at the standard conditions $T = T_{ref} = 293.15K$ and $p_i = 1 atm$, it can be shown that

$$\frac{\hat{h}_i(T)}{R_u} = a_{i5} + \sum_{\ell=0}^4 \frac{a_{i\ell}}{\ell+1} T^{\ell+1} \quad (2.96)$$

Here

$$a_{i5} \stackrel{\text{def}}{=} \frac{\hat{h}_{fi}}{R_u} - \sum_{\ell=0}^4 \frac{a_{i\ell}}{\ell+1} (T_{ref})^{\ell+1} \quad (2.97)$$

can also be found in NASA CEA Program. As such \hat{h}_i can be evaluated using Eq. (2.96). In turn, h_i and e_i can be evaluated using the relations (i) $h_i = \hat{h}_i / M_i$ and (ii) $e_i \equiv h_i - p_i / \rho_i = h_i - R_i T$.

Next, by using (i) Eqs. (2.1) and (2.93), (ii) $R_u = M_i R_i$, and (iii) the thermodynamic relation $T ds_i = dh_i - dp_i / \rho_i$, one concludes that

$$d\hat{s}_i = \frac{d\hat{h}_i}{T} - R_u \frac{dp_i}{p_i} \quad (2.98)$$

Let \hat{s}_i^0 denotes the value of \hat{s}_i at p_i atm. Then $\hat{s}_i^0 = \hat{s}_i^0(T)$ and Eq. (2.98) implies that

$$\hat{s}_i^0(T) = \int_{T_{ref}}^T \frac{\hat{c}_{pi}(T')}{T'} dT' + \hat{s}_i^0(T_{ref}) \quad (2.99)$$

By using Eqs. (2.94) and (2.99), it can be shown that

$$\frac{\hat{s}_i^0(T)}{R_u} = a_{i6} + a_{i0} \ln T + \sum_{\ell=0}^4 \frac{a_{i\ell}}{\ell} T^{\ell} \quad (2.100)$$

where

$$a_{i6} \stackrel{\text{def}}{=} \frac{\hat{s}_i^0(T_{ref})}{R_u} - a_{i0} \ln T_{ref} - \sum_{\ell=0}^4 \frac{a_{i\ell}}{\ell} (T_{ref})^{\ell} \quad (2.101)$$

can be found in NASA CEA Program. As such \hat{s}_i^0 can be evaluated using Eq. (2.100).

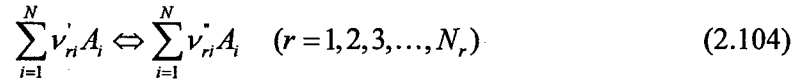
Let $\hat{h}_i^0(T)$ and $\hat{g}_i^0(T)$, respectively, denote the molar specific enthalpy and the molar specific Gibbs free energy of species i at the temperature T and the pressure = 1 atm. Then, by definition,

$$\hat{g}_i^0(T) = \hat{h}_i^0(T) - T\hat{s}_i^0(T) \quad (2.102)$$

Because \hat{h}_i is assumed to be independent of pressure, $\hat{h}_i^0(T) = \hat{h}_i(T)$ in current study. Thus, with the aid of Eqs. (2.96) and (2.100), Eq. (2.102) implies that

$$\frac{\hat{g}_i^0(T)}{R_u T} = \frac{a_{i5}}{T} + (a_{i0} - a_{i6}) - a_{i0} \ln T - \sum_{\ell=0}^4 \frac{a_{i\ell}}{\ell(\ell+1)} (T)^\ell \quad (2.103)$$

To proceed, a set of Nr chemical reactions involving N chemical species is represented by the following reaction equations:



Here (i) A_i denote the i th chemical species, and (ii) ν'_{ri} and ν''_{ri} , respectively, denote the stoichiometric coefficients of reactants and products for species i in the r th reaction. Let (i) K_{fr} and K_{br} , respectively, denote the forward (i.e., left to right) and the backward (i.e., right to left) reaction rate constants of the r th reaction; (ii) $n_i = \rho_i / M_i$ = the molar concentration (moles per unit volume) of species i ; and (iii) $(\dot{n}_i)_r$ denote the molar generation rate (moles per unit time and per unit volume) of species i contributed by the r th reaction. Then the law of mass action implies that

$$(\dot{n}_i)_r = (\nu''_{ri} - \nu'_{ri}) \left(K_{fr} \prod_{\ell=1}^N (n_\ell)^{\nu'_{\ell r}} - K_{br} \prod_{\ell=1}^N (n_\ell)^{\nu''_{\ell r}} \right) \quad (2.105)$$

Here K_{fr} and K_{br} can be evaluated using the Arrhenius forms, i.e.,

$$K_{fr}(T) = A_{fr} T^{B_{fr}} \exp\left(-\frac{E_{fr}}{R_u T}\right) \text{ and } K_{br}(T) = A_{br} T^{B_{br}} \exp\left(-\frac{E_{br}}{R_u T}\right) \quad (2.106)$$

with A_{fr} , A_{br} , B_{fr} , B_{br} , E_{fr} , and E_{br} being given constant coefficients. The values of these coefficients for some chemical reactions are tabulated in Appendices I and II.

If the kinetic data of the backward reactions were not available, K_{br} may be evaluated using the relation

$$K_{br} = K_{fr} / K_{eqr} \quad (2.107)$$

where K_{eqr} , the equilibrium constant for the r th reaction, is a function of T and can be evaluated using the relation

$$K_{eqr}(T) = \left(\frac{1}{R_u T} \right)^{\sum_{i=1}^N (\nu_{ri}^* - \nu_{ri}')} \exp \left[- \sum_{i=1}^N (\nu_{ri}^* - \nu_{ri}') \frac{\hat{g}_i^0(T)}{R_u T} \right] \quad (2.108)$$

Next, with the aid of Eq. (2.105) and the relations: (i)

$$\dot{\omega}_i = M_i \sum_{r=1}^{N_r} (\dot{n}_i)_r \quad (2.109)$$

(ii) $n_i = \rho_i / M_i$, and (iii) $K_{fr} = K_{fr}(T)$ and $K_{br} = K_{br}(T)$, $r = 1, 2, \dots, N_r$, each $\dot{\omega}_i$ can be explicitly expressed as a function of $\rho_1, \rho_2, \dots, \rho_N$ and T , i.e.,

$$\dot{\omega}_i = M_i \sum_{r=1}^{N_r} (\nu_{ri}^* - \nu_{ri}') \left[K_{fr}(T) \prod_{\ell=1}^N \left(\frac{\rho_\ell}{M_\ell} \right)^{\nu_{r\ell}'} - K_{br}(T) \prod_{\ell=1}^N \left(\frac{\rho_\ell}{M_\ell} \right)^{\nu_{r\ell}^*} \right] \quad (2.110)$$

As will be shown shortly, alternatively each $\dot{\omega}_i$ can also be considered as an implicit function of the conservative variables u_m , $m = 1, 2, \dots, N+2$. In fact, evaluation of $\partial \dot{\omega}_i / \partial u_m$ for all $i = 1, 2, \dots, N-1$ and $m = 4, 5, \dots, N+2$ is required for a later application. As such, in the remainder of this section these derivatives will be expressed explicitly in terms of a set of flow and thermodynamic variables.

To proceed, first Eq. (2.110) is used to obtain

$$\frac{\partial \dot{\omega}_i}{\partial \rho_k} = M_i \sum_{r=1}^{N_r} (\nu_{ri}^* - \nu_{ri}') \left[\frac{K_{fr} \nu_{rk}'}{\rho_k} \prod_{\ell=1}^N (n_\ell)^{\nu_{r\ell}'} - \frac{K_{br} \nu_{rk}^*}{\rho_k} \prod_{\ell=1}^N (n_\ell)^{\nu_{r\ell}^*} \right], \quad i, k = 1, 2, \dots, N \quad (2.111)$$

and

$$\frac{\partial \dot{\omega}_i}{\partial T} = M_i \sum_{r=1}^{N_r} (\nu_{ri}^* - \nu_{ri}') \left[\dot{K}_{fr} \prod_{\ell=1}^N (n_\ell)^{\nu_{r\ell}'} - \dot{K}_{br} \prod_{\ell=1}^N (n_\ell)^{\nu_{r\ell}^*} \right], \quad i = 1, 2, \dots, N \quad (2.112)$$

with

$$\dot{K}_{fr} \stackrel{\text{def}}{=} \frac{dK_{fr}(T)}{dT} \quad \text{and} \quad \dot{K}_{br} \stackrel{\text{def}}{=} \frac{dK_{br}(T)}{dT} \quad (2.113)$$

Here (i) each $\partial \dot{\omega}_i / \partial \rho_k$ is evaluated assuming that, except ρ_k , all other independent variables in the set $\{\rho_1, \rho_2, \dots, \rho_N, T\}$ are held constant; and (ii) each $\partial \dot{\omega}_i / \partial T$ is evaluated assuming that $\rho_1, \rho_2, \dots, \rho_N$ are held constant.

Next, because (i) $\rho_i = u_{3+i}$, $i = 1, 2, \dots, N-1$, and (ii) $\rho_N = \rho - \sum_{\ell=1}^{N-1} \rho_\ell = u_1 - \sum_{\ell=1}^{N-1} u_\ell$, one has

$$\frac{\partial \rho_i}{\partial u_m} = \delta_m^{3+i}, \quad i = 1, 2, \dots, N-1; \quad m = 1, 2, \dots, N+2 \quad (2.114)$$

and

$$\frac{\partial \rho_N}{\partial u_m} = \begin{cases} 1 & \text{if } m = 1 \\ 0 & \text{if } m = 2, 3 \\ -1 & \text{if } m = 4, 5, \dots, N+2 \end{cases} \quad (2.115)$$

Here, as in earlier cases, any partial derivative with respect to any conservative variable u_m is evaluated assuming that, except u_m , all other variables in the set $\{u_1, u_2, \dots, u_{N+2}\}$ are held constant.

Next, with the aid of Eq. (2.35), the first equation in Eq. (2.40) implies that

$$de = \frac{1}{\rho} \left[(u^2 - E) du_1 - u du_2 + du_3 \right] \quad (2.116)$$

Also, with the aid of Eqs. (2.13) and (2.33), Eqs. (2.16) and (2.116) imply that

$$dT = \frac{1}{\rho c_v} \left[\left(\frac{u^2}{2} - e_N \right) du_1 - u du_2 + du_3 - \sum_{m=4}^{N+2} (e_{m-3} - e_N) du_m \right] \quad (2.117)$$

Eqs. (2.117) implies that T is an implicit function of u_1, u_2, \dots, u_{N+2} with

$$\frac{\partial T}{\partial u_1} = \frac{1}{\rho c_v} \left(\frac{u^2}{2} - e_N \right), \quad \frac{\partial T}{\partial u_2} = -\frac{u}{\rho c_v} \quad \text{and} \quad \frac{\partial T}{\partial u_3} = \frac{1}{\rho c_v} \quad (2.118)$$

and

$$\frac{\partial T}{\partial u_m} = \frac{e_N - e_{m-3}}{\rho c_v}, \quad m = 4, 5, \dots, N+2 \quad (2.119)$$

Note that: (i) each $\dot{\omega}_i$ is a function of the independent variables $\rho_1, \rho_2, \dots, \rho_N$, and T , and (ii) the independent variables themselves are functions of u_m , $m = 1, 2, \dots, N+2$. Thus each $\dot{\omega}_i$ can also be considered as a function of u_m , $m = 1, 2, \dots, N+2$. Moreover, by using the chain rule, each

$\partial \dot{\omega}_i / \partial u_m$ ($i = 1, 2, \dots, N$ and $m = 1, 2, \dots, N+2$) can be obtained with the aid of Eqs. (2.111), (2.112), (2.118), and (2.119). In particular, for $i = 1, 2, \dots, N-1$ and $m = 4, 5, \dots, N+2$, one has

$$\begin{aligned}
 \frac{\partial \dot{\omega}_i}{\partial u_m} &= \sum_{k=1}^{N-1} \frac{\partial \dot{\omega}_i}{\partial \rho_k} \frac{\partial \rho_k}{\partial u_m} + \frac{\partial \dot{\omega}_i}{\partial \rho_N} \frac{\partial \rho_N}{\partial u_m} + \frac{\partial \dot{\omega}_i}{\partial T} \frac{\partial T}{\partial u_m} \\
 &= \frac{\partial \dot{\omega}_i}{\partial \rho_{m-3}} - \frac{\partial \dot{\omega}_i}{\partial \rho_N} + \frac{\partial \dot{\omega}_i}{\partial T} \left(\frac{e_N - e_{m-3}}{\rho c_v} \right) \\
 &= M_i \sum_{r=1}^{N_r} (\dot{v}_{ri} - \dot{v}_{ri}') \left[K_{fr} \left(\frac{\dot{v}_{r(m-3)}}{\rho_{m-3}} - \frac{\dot{v}_{rN}}{\rho_N} \right) \prod_{\ell=1}^N (n\ell)^{\dot{v}_{ri}'} \right. \\
 &\quad \left. - K_{br} \left(\frac{\dot{v}_{r(m-3)}}{\rho_{m-3}} - \frac{\dot{v}_{rN}}{\rho_N} \right) \prod_{\ell=1}^N (n\ell)^{\dot{v}_{ri}} \right] \\
 &\quad + M_i \left(\frac{e_N - e_{m-3}}{\rho c_v} \right) \sum_{r=1}^{N_r} (\dot{v}_{ri} - \dot{v}_{ri}') \left[\dot{K}_{fr} \prod_{\ell=1}^N (n\ell)^{\dot{v}_{ri}'} - \dot{K}_{br} \prod_{\ell=1}^N (n\ell)^{\dot{v}_{ri}} \right] \\
 &\quad i = 1, 2, \dots, N-1; \quad m = 4, 5, \dots, N+2
 \end{aligned} \tag{2.120}$$

2.5 Flow Equations in Multi-Dimensional Space

In the past, the fundamental behavior of cavity flows was known as two-dimensional [8]. Equation (2.121) shows the vector form of the two-dimensional flow equations in Cartesian coordinates, including the continuity equation, the Navier-Stokes equations, the energy equation, and one species equation:

$$\frac{\partial \mathbf{U}}{\partial t} + \frac{\partial \mathbf{F}}{\partial x} + \frac{\partial \mathbf{G}}{\partial y} - \frac{\partial \mathbf{F}_v}{\partial x} - \frac{\partial \mathbf{G}_v}{\partial y} = 0 \tag{2.121}$$

where the flow variable vector

$$\mathbf{U} = \begin{pmatrix} \rho \\ \rho u \\ \rho v \\ \rho e \\ \rho Y_f \end{pmatrix},$$

the inviscid flux vectors are

$$\mathbf{F} = \begin{pmatrix} \rho u \\ \rho u^2 + p \\ \rho uv \\ u(\rho e + p) \\ \rho u Y_f \end{pmatrix},$$

$$\mathbf{G} = \begin{pmatrix} \rho v \\ \rho uv \\ \rho v^2 + p \\ v(\rho e + p) \\ \rho v Y_f \end{pmatrix},$$

and the viscous flux vectors are

$$\mathbf{F}_v = \begin{pmatrix} 0 \\ \tau_{xx} \\ \tau_{xy} \\ u\tau_{xx} + v\tau_{xy} - q_x \\ -\rho \hat{u}_f Y_f \end{pmatrix},$$

$$\mathbf{G}_v = \begin{pmatrix} 0 \\ \tau_{xy} \\ \tau_{yy} \\ u\tau_{xy} + v\tau_{yy} - q_y \\ -\rho \hat{v}_f Y_f \end{pmatrix}.$$

In the above equations, ρ is the density; u and v are velocity components in the x and the y directions, respectively; p is the static pressure; $e = \varepsilon + \frac{1}{2}(u^2 + v^2)$ is the specific total energy with ε as the specific internal energy. We assume the fluid is ideal and polytropic. Due to the equation of state of an ideal gas, $p = (\gamma - 1)\rho \varepsilon$, where $\gamma = C_p/C_v$ is the specific heat ratio and it is a constant due to the polytropic gas assumption. In the viscous vectors, τ_{xx} , τ_{xy} , and τ_{yy} are stress components, and q_x and q_y are the heat conduction fluxes in x and y directions, respectively. Y_f is the mass fraction of fuel. The diffusion velocity components, \hat{u} and \hat{v} are calculated by Fick's law:

$$Y_f \hat{u}_f = -D \frac{\partial Y_f}{\partial x}, \quad (2.122a)$$

$$Y_f \hat{v}_f = -D \frac{\partial Y_f}{\partial y}, \quad (2.122b)$$

where D is the mass diffusivity of fuel in the gas mixture. The molecular viscosity μ is calculated using Sutherland's law [12] and the Lewis number $Le=1$ is assumed to calculate the mass diffusivity D . In numerical calculations, the above governing equations are nondimensionalized by the free stream conditions, i.e., velocity components by u_∞ , density by ρ_∞ , pressure by $\rho_\infty u_\infty^2$, and the total energy by $\rho_\infty u_\infty^2$. The subscript ∞ denotes the free stream condition. The cavity depth d is used as the length scale, and the time scale is d/u_∞ .

3. The CESE Method

The CESE method is a novel numerical framework for high-fidelity solution of hyperbolic conservation laws. Originally developed by Chang and coworkers [13-18], the tenet of the CESE method is a unified treatment of space and time in calculating flux balance. Contrast to modern upwind schemes, no Riemann solver and/or a reconstruction procedure is used as the building block of the CESE method. As a result, the logic and computational counts of the CESE method are simpler and more efficient. Based on the CESE method, computer programs for solving unsteady flows in one, two, and three spatial dimensions for structured, and unstructured meshes, and for meshes composed of mixed elements have been developed. These solvers have been parallelized based on domain decomposition in conjunction of the use of MPI. Since no Riemann solver is used, we have straightforwardly extended the CESE method for flows with complex physical processes, including detonation, cavitations, and MHD.

Previously, various flow phenomena have been calculated by using the CESE method. In particular, the CESE solver is capable of calculating high-speed compressible flow as well as flows at very low Mach numbers without applying preconditioning to the governing equations. The CESE method is indeed an all speed solver. Moreover, the CESE method is capable of simultaneously capture strong shock waves and the acoustic waves in the same computational domain, while the amplitude of the pressure jump across the shock wave would be several orders of magnitude higher than that of the acoustic waves.

The CESE method employed in the present paper is based on the use of quadrilateral cells on the x-y plane [17], which was extended from the original CESE method. Note that the original CESE method for two-dimensional flows was designed based on the use of triangular cells. In the present paper, a brief discussion of this particular extension of the CESE method is provided. The discussions here will be focused on the space-time geometry of the CESE method. We remark that the basic structure of the CESE method can always be easily grasped by visualizing the space-time geometry of conservation element (CE), solution element (SE), and how they facilitate the space-time integration. The detailed algebraic equations of the method, perhaps, only reaffirm the structure of the method. We of course refer the interested readers to the cited references for all details.

To proceed, let E_3 denote a three-dimensional Euclidean space, in which $x_1 = x$, $x_2 = y$, and $x_3 = t$. Let $\nabla \cdot$ be the divergence operator in E_3 , and $\mathbf{h}_m \stackrel{\text{def}}{=} [(f - f_v)_m, (g - g_v)_m, u_m]$ for $m=1, 2, 3, 4$, and 5 . Here $(f - f_v)_m$, $(g - g_v)_m$, and u_m are the m^{th} components of $\mathbf{F} - \mathbf{F}_v$, $\mathbf{G} - \mathbf{G}_v$, and U , respectively, in Eq. (1). Aided by the above definition, for each $m=1, 2, \dots, 5$, the flow equations, Eq. (1), becomes

$$\nabla \cdot \mathbf{h}_m = 0, \quad (3.1a)$$

Apply Gauss's divergence theorem to Eq. (3a) and we get

$$\oint_{S(V)} \mathbf{h}_m \cdot d\mathbf{s} = 0, \quad (3.1b)$$

As depicted in Fig. 1(a), $S(V)$ is the boundary of the space-time region V in E_3 and $d\mathbf{s}$ is a surface element vector pointing outward. Equation (3b) states that the total space-time flux \mathbf{h}_m leaving volume V through $S(V)$ vanishes. All mathematical operations can be carried out as though E_3 were an ordinary three-dimensional Euclidean space. The CESE method is designed to accurately integrate Eq. (3b) to provide high fidelity results of evolving u_m in the space-time domain.

The CESE method is a family of numerical schemes, with the α scheme [13] as its backbone. Contrast to conventional finite volume methods, the CESE method has separate definitions of conservation element (CE) and solution element (SE) in constructing the discretized equations for integrating Eq. (3b) in the space-time domain. CEs are non-overlapping space-time sub-domains such that (i) the whole computational domain can be filled by the CEs; (ii) flux conservation can be enforced over each CE and/or over a union of several neighboring CEs; and (iii) inside a CE, flow discontinuity is allowed. On the other hand, SEs are non-overlapping space-time sub-domains such that (i) SEs do not generally coincide with a CE; (ii) the union of all SEs does not have to fill the whole computational domain; (iii) flow variables and fluxes are discontinuous across interfaces of neighboring SEs; and (iv) within a SE, flow variable and flux function are assumed continuous and they are approximated by using a prescribed smooth function. In the present paper, a first-order Taylor series expansion is used. Thus the discretized flow variables and fluxes are linearly distributed inside each SE.

The time marching strategy in the CESE method is designed based on a space-time staggered mesh stencil composed of CEs and SEs. Note that when integrating Eq. (3b) over the boundary of a CE, the surface element of $S(V)$ in Eq. (3b) always lying inside a SE, where flow variables

and fluxes are continuous. We remark that the paradigm of the Godunov schemes is that one has to resort to the use of a Riemann solver to reckon the nonlinear flux function at the cell interfaces. In the CESE method, however, flow information propagates only in one direction across all cell interfaces, i.e., towards future. Thus, the space-time flux integration can be straightforwardly carried out without reconciling the values of flux functions at cell interfaces through the use of a Riemann solver. In other words, contrast to the upwind methods, there is no cell interface, across which two way traffics of flow information propagate. Thus, the CESE method can capture shocks without using a Riemann solver. In what follows, we discuss specific space-time geometry of the CE and SE in integrating Eq. (3b).

Consider Fig. 1(b). The x - y plane is divided into non-overlapping quadrilaterals. Two neighboring quadrilaterals share a common side. Vertices and centroids of quadrilaterals are marked by dots and circles, respectively. Q is the centroid of the quadrilateral $B_1B_2B_3B_4$. A_1 , A_2 , A_3 , and A_4 , respectively, are the centroids of the four quadrilaterals neighboring to the quadrilateral $B_1B_2B_3B_4$. Q^* , marked by a cross in Fig. 1(b), is the centroid of the polygon $A_1B_1A_2B_2A_3B_3A_4B_4$. Hereafter, point Q^* , which generally does not coincide with point Q , is referred to as the solution point associated with Q . Note that points A_1^* , A_2^* , A_3^* , and A_4^* , which are also marked by crosses, are the solution points associated with the centroids A_1 , A_2 , A_3 , and A_4 , respectively.

To proceed, we consider Fig. 1(c). Here $t = n\Delta t$ at the n th time level, where $n = 0, 1/2, 1, 3/2, \dots$. For a given $n > 0$, Q , Q' , and Q'' , respectively, denote the points on the n^{th} , the $(1-1/2n)^{\text{th}}$, and $(1+1/2n)^{\text{th}}$ time levels with point Q being their common spatial projection. Other space-time mesh points, such as those depicted in Fig. 1(c), and also those not depicted, are defined similarly. In particular, Q^* , A_1^* , A_2^* , A_3^* , and A_4^* lie on the n th time level and they are the space-time solution mesh points associated with points Q , A_1 , A_2 , A_3 , and A_4 . Q'' , A_1'' , A_2'' , A_3'' , and A_4'' lie on the $(1-1/2n)^{\text{th}}$ time level and are the space-time solution mesh points associated with points Q' , A_1' , A_2' , A_3' , and A_4' .

With the above preliminaries, we are ready to discuss the geometry of the CE and SE associated with point Q^* , where the numerical solution of the flow variables u_m at n th time level are calculated based on the known flow solution in all points at a previous time level, i.e., $n-1/2$, denoted by superscript prime. First, the solution element of point Q^* , denoted by $SE(Q^*)$, is

defined as the union of the five plane segments $Q'Q''B_1B_1'$, $Q'Q''B_2B_2'$, $Q'Q''B_3B_3'$, $Q'Q''B_4B_4'$, and $A_1B_1A_2B_2A_3B_3A_4B_4$ and their immediate neighborhoods.

To integrate Eq. (3b), four basic conservation elements (BCEs) of point Q^* are constructed, and they are denoted by $BCE_l(Q)$, with $l = 1, 2, 3$, and 4 . These four BCEs are defined to be the space-time cylinders $A_1B_1QB_4A_1'B_1'Q'B_4'$, $A_2B_2QB_1A_2'B_2'Q'B_1'$, $A_3B_3QB_2A_3'B_3'Q'B_2'$, and $A_4B_4QB_3A_4'B_4'Q'B_3'$, respectively. In addition, the compounded conservation element of point Q , denoted by $CE(Q)$, is defined to be the space-time cylinder $A_1B_1A_2B_2A_3B_3A_4B_4A_1'B_1'A_2'B_2'A_3'B_3'A_4'B_4'$, i.e., the union of the above four BCEs.

To proceed, the set of the space-time mesh points whose spatial projections are the centroids of quadrilaterals depicted in Fig. 1(b) is denoted by Ω and the set of the space-time mesh points whose spatial projections are the solution points depicted in Fig. 1(b) is denoted by Ω^* . Note that the BCEs and the compounded CE of any mesh point $\in \Omega$ and the SE of any mesh point $\in \Omega^*$ are defined in a manner identical to that described earlier for point Q and Q^* . With the clear definitions of the CE and SE in above, the numerical integration of the space-time flux balance, i.e., Eq. (3b), in the present modified CESE method can be summarized as follows.

For any $Q^* \in \Omega^*$ and $(x, y, t) \in SE(\Omega^*)$, the flow variables and flux vectors, i.e., $u_m(x, y, t)$, $f_m(x, y, t)$, and $g_m(x, y, t)$, are approximated to their numerical counterparts, i.e., $u_m^*(x, y, t)$, $f_m^*(x, y, t)$, and $g_m^*(x, y, t)$, by using the first order Taylor series expansion with respect to $Q^* (x_{Q^*}, y_{Q^*}, t^*)$. Thus the space-time flux vector $\mathbf{h}_m(x, y, t)$, can be replaced by $\mathbf{h}_m^*(x, y, t; Q^*)$ and the numerical analogue of Eq. (3b) for each $m=1,2,\dots,5$, is

$$\oint_{S(CE(Q))} \mathbf{h}_m^* \cdot d\mathbf{s} = 0, \quad (3.2)$$

Equation (3.2) states that the discretized total flux of \mathbf{h}_m^* leaving $CE(Q)$ through its boundary vanishes. We note that Eq. (4) can be written in terms of independent discrete solution variables which are the main flow variables and their spatial derivatives, $(u_{mx})_{Q^*}$ and $(u_{my})_{Q^*}$ in this approximation process.

By conducting the integration of Eq. (4) over the CE= BCE₁+BCE₂+BCE₃+BCE₄, the discrete flow variables $(u_m)_{Q^*}$ associated with the space-time point Q^* , can be straightforwardly evaluated. This is achieved by the aid of the geometrical information of CE(Q^*) as shown in Fig. 1, and the linear distribution of $(u_m)_{Q^*}$ in each SE due to the adopted first-order Taylor series expansion for the flow variables inside the SE as the discretization process.

The calculation of the gradient variables, i.e., $(u_{mx})_{Q^*}$, and $(u_{my})_{Q^*}$ is base on a finite-difference approach in conjunction with the standard CESE artificial damping functions, i.e., the a- ε - α scheme, in which parameter ε is associated with the overall damping effect and α is for shock capturing. In contrast to the original CESE method, the calculation of $(u_{mx})_{Q^*}$, and $(u_{my})_{Q^*}$ has nothing to do with the space-time flux conservation.

To calculate unsteady flows, the non-reflecting boundary condition treatment is critically important. Without an effective treatment, the reflected waves would inevitably contaminate the evolving flow solutions. Numerical treatments to achieve non-reflecting boundary condition in the setting of conventional CFD methods have been an active research subject for a long time. In general, most of treatments were developed based on theorems of the partial differential equation, and they could be categorized into the following three groups: (i) applying the method of characteristics to the discretized equations, (ii) the use of the buffer zone or a perfectly matched layer, and (iii) applying asymptotic analytical solution at the far field.

In the setting of the CESE method, we only concern the integral equation. The above ideas of treating non-reflective boundary are not applicable. Instead, the non-reflecting boundary condition treatments in the setting of the CESE method is based on flux conservation in the vicinity of the computational boundary [18]. In other words, the present nonreflecting boundary condition treatment is equivalent to letting the incoming flux from the interior domain to the boundary CE smoothly exit to the exterior of the domain. In the setting of the CESE method, the numerical implementation of this flux-based method is extremely simple due to the fact that all flow information must propagate into the future. Chang and coworkers [18] have provided detailed discussions of various implementations of the above principle. It

has been demonstrated that only negligible reflection occurs when a shock passes through the domain boundary. Moreover, along a wall boundary, a unified boundary condition for viscous flows is used. Based on local space-time flux conservation, a no-slip condition will be automatically enforced when the viscosity is not null. Again, the basic principle is based on the space-time flux conservation over CEs near the computational boundary.

4. Results and Discussions

Three sets of numerical results are presented: (i) supersonic cavity flow in the supersonic combustion facility by Gruber et al. [1, 2] and Baurle et al. [5], (ii) Stalling and Wilcox's cavity flow test [20], and (iii) cavity flows with fuel injection. The first test is to assess numerical accuracy of the calculated frequencies. The results will be compared with previously reported data and Rossiter's empirical relation [6]. The second test is to assess numerical accuracy of time-averaged amplitudes of pressure fluctuations along the cavity walls. The results will be compared with the experimental data [20]. In the third test, cavity flows with downstream as well as upstream injections are simulated. We will show that a cavity flow with a downstream transverse injection can effectively generate strong vortices and acoustic waves for fuel/air mixing enhancement.

4.1 Frequency Calculations

The first numerical example follows the testing condition in the US AFRL supersonic combustion facility reported in [1, 2, 5]. A supersonic flow at Mach 2 and Reynolds number of 4×10^5 passes a swallow cavity with $L/d = 7.76$, where L and d are the length and depth of the cavity, respectively. The computational domain outside of the cavity is $0 \leq x \leq 11.52$, and $0 \leq y \leq 3.82$, where x and y are nondimensionalized by d . Mesh points were clustered at the forward and aft bulkheads, at the plane spanning over the cavity mouth, and along the lateral sidewalls of the cavity. 143,000 quadrilateral elements are used for the computational domain. Figure 2 shows the mesh, in which one of every five mesh lines is displayed. The non-reflecting boundary condition is applied to the free stream surfaces and outlet. Initially, velocities inside the cavity are set to zero, and the density and pressure of the whole domain are set to the free stream values. The time step was chosen such that $CFL \approx 0.8$ based on the free stream condition.

Figure 3 shows a series of snapshots of pressure contours, vorticity contours, and numerical Schlieren images, which are contour plots of

$$|\nabla \rho| = \sqrt{\left(\frac{\partial \rho}{\partial x}\right)^2 + \left(\frac{\partial \rho}{\partial y}\right)^2}. \quad (4.1)$$

These figures demonstrate very complex flow features, including traveling acoustic waves, vortex generation at the leading edge, shedding vortices in the free shear layer, and pressure waves impinging on and rebounding from the aft wall. The interactions between the rebounding pressure waves and shed vortices form a feed back loop which leads to self-sustained oscillations as illustrated by Rossiter [6]. In Fig. 3(b), periodic shear layer deflections in the transverse direction could be clearly discerned. Inward deflection results in mass addition into the cavity; outward deflection expels mass from the cavity. This periodic mass addition/expulsion mechanism enhances fuel/air mixing. Moreover, flapping shock/expansion waves emanating from the upstream bulkhead of the cavity, shown in Fig. 3(c), can also enhance fuel/air mixing.

Figure 4 shows pressure histories on the aft wall and on the floor. The flow has reached a self-sustained oscillatory state after about $15 t_c$, where $t_c = d / U_\infty$. However, the oscillation pattern changes from cycle to cycle, and we cannot clearly identify the period of the oscillation cycles. This is consistent with experimental observation reported in [19]. The amplitude of the pressure oscillations at the aft wall is much higher than that at the cavity floor due to the mass addition/expulsion mechanism near the aft wall. Figure 5 shows the frequency spectra of the pressure data in Fig. 4. The predicted values of the dominant frequencies compare well with the Rossiter relation [6] and the numerical results by Baurle et al. [5]. The Rossiter formula is

$$f_m = \frac{U}{L} \left(1 - \frac{m}{M} \right) / \frac{1}{2} \quad (4.2)$$

where f_m is the resonant frequency corresponding to the m th mode, U is the main stream velocity, L is the cavity length, $\theta = 0.513$, and $K = 0.57$ [5]. Figure 5 shows five calculated dominant frequencies, i.e., 2523, 3533, 4290, 5804, and 8579Hz, compare well with the 3rd, 4th, 5th, 6th, and 9th mode predicted by the Rossiter relation. The first and second frequency modes also compared well with Baurle's calculation.

To proceed, we perform simulation of the same cavity flow with an added transverse injection at upstream of the cavity. The free stream flow condition and the cavity geometry are identical to that shown in Figs. 3-5. The injection jet opening is 0.2 d , and its center is located 1.0 d upstream from the leading edge of the cavity. A choked jet with a uniform condition at the opening is imposed: